High-Gain On-Chip Antenna Design on Silicon Layer with Aperture Excitation for Terahertz Applications

Mohammad Alibakhshikenari, *Member IEEE,* Bal S. Virdee, *Senior Member IEEE,* Mohsen Khalily, *Senior Member IEEE*, Chan H. See, *Senior Member IEEE,* Raed Abd-Alhameed, *Senior Member IEEE,* Francisco Falcone, *Senior Member IEEE,* Tayeb A. Denidni, *Fellow IEEE*, and Ernesto Limiti, *Senior Member IEEE*

***Abstract*— This article investigates the feasibility of designing a wideband high-gain on-chip antenna on silicon technology for sub-terahertz applications. High-gain is achieved by exciting the antenna using an aperture fed mechanism to couple electromagnetics energy from a metal slot-line, which is sandwiched between the silicon and polycarbonate substrates, to a 15-element array comprising circular and rectangular radiation patches fabricated on the top surface of the polycarbonate layer. An open ended microstrip line, which is orthogonal to the metal slot-line, is implemented on the underside of the silicon substrate. When the open ended microstrip line is excited it couples the signal to the metal slot-line which is subsequently coupled and radiated by the patch array. Measured results show the proposed on-chip antenna exhibits a reflection coefficient of less than -10 dB across 0.290 THz to 0.316 THz with a highest gain and radiation efficiency of 11.71 dBi and 70.8%, respectively. The antenna has a very narrow stopband between 0.292 THz to 0.294 THz. The physical size of the presented sub-terahertz on-chip antenna is 20×3.5×0.126 mm^3.**

***Index Terms*— Terahertz (THz) On-chip antenna, coupling feeding mechanism, integrated circuit, high gain, silicon technology, broad bandwidth.**

I. Introduction

Recent technological advances have established possible the generation and discovery of Terahertz (THz) radiation [1-6]. This has resulted in a formerly inaccessible zone of the electromagnetic (EM) spectrum attainable, which is a territory of large potential for medical imaging and radio astronomy. Characteristics of the THz band permit it to occupy a unique niche as other parts of the EM spectrum are already well established [7-9]. One of the main obstacles encountered in realizing a commercial THz system is the high path-loss and atmospheric attenuation incurred by the signal [10,11]. This necessitates high-gain transmit and receive THz antennas. Typical THz antennas include a lens antenna which is combined of an expanded hemispherical silicon lens [12], and a diagonal multilayer horn [13]. Although these types of antennas provide high gain up to 12.5 dB however, they are bulky structures that limits their applications.

In this research work, the viability of an on-chip antenna has been demonstrated to offer wide frequency range and high-gain performance across 0.290 THz to 0.316 THz with a narrow stopband between 0.292 THz to 0.294 THz. High-gain performance is achieved by employing an aperture feed mechanism whereby THz electromagnetic energy is coupled from an open ended microstrip-line via a metal slot-line to the radiation patch array with minimal loss. The antenna is fabricated on low permittivity THz substrate and on silicon technology. The proposed THz antenna for on-chip integration is simple to design and implement, and furthermore a low-profile structure.

II. Design Procedure of the On-Chip Antenna Excited with a Innovative Feeding Structure

Fig.1 displays the 3-D vision of the proposed sub-THz on-chip antenna. The antenna includes of a periodic array of 15 radiating elements fabricated on the top surface of a polycarbonate layer. Each radiating element comprises a rectangular patch and a circular patch. Dimension of the rectangular patch is 2.8×0.2 mm^2, and the circular patch has a radius of 0.25 mm. Gap between the center of the two patches is 0.6 mm. Spacing between adjacent pairs of patches is 0.25 mm, which corresponds to the guided wavelength of the metal slot-line at 0.3 THz, thus ensuring the field distribution is uniform over the aperture of the antenna.

The antenna array is fed serially through the open-circuited conductive slot-line with length and width of l = 19 mm and w = 0.16 mm, which is embedded in the high resistivity intrinsic silicon-substrate layer with a relative permittivity of ε_r=11.9, tanδ=0.00025, and a thickness of h_1=70 μm. Polycarbonate substrate is used to support the radiation patches. It has a relative permittivity of ε_r=2.1, tanδ=0.01 and a thickness of h_2=50 μm. The silicon and polycarbonate substrates were bonded together using thermal compression. Silicon is a low-thermal-expansion material however polycarbonate can experience thermal stresses during the annealing treatment which can induce fracturing in the polycarbonate substrate. It was found that by limiting the maximum annealing temperature the fracturing can be avoided. The metallization

M. Alibakhshikenari and E. Limiti are with Electronic Eng. Dep., University of Rome "Tor Vergata", Via del Politecnico 1, 00133, Rome, ITALY (e-mail: alibakhshikenari, limiti@ing.uniroma2.it).

B. S. Virdee, is with London Metropolitan University, Center for Communications Technology, London N7 8DB, UK (e-mail: b.virdee@londonmet.ac.uk).

M. Khalily is with Institute for Communication Systems (ICS), Home of 5G Innovation Centre (5GIC), University of Surrey, Guildford, UK, GU2 7XH (e-mail: m.khalily@surrey.ac.uk).

C. H. See was with School of Eng., University of Bolton, Deane Road, Bolton, BL3 5AB, UK. He is now with the School of Eng. and the Built Environment, Edinburgh Napier University, 10 Colinton Road, Edinburgh, EH10 5DT, UK (e-mail: c.see@napier.ac.uk).

R. Abd-Alhameed is with School of Electrical Eng. & Computer Science, University of Bradford, Bradford, BD7 1DP, UK (e-mail: r.a.a.abd@bradford.ac.uk).

F. Falcone is with Electric and Electronic Eng. Dep., Universidad Pública de Navarra, SPAIN (e-mail: francisco.falcone @unavarra.es).

T. A. Denidni is with Institut National de la Recherche Scientifique (INRS), Université du Quebec, Montreal, QC, CANADA (e-mail: denidni@emt.inrs.ca).

layer was created using sputter deposition process. The feed mechanism proposed here to excite the array is realized using an open-ended microstrip line which is implemented on the underside of the silicon-layer and is orthogonally arranged relative to the metal slot-line. Dimensions of the open-circuited microstrip-line are 2.8×0.2 mm^2. The conductive slot-line is embedded on the top-surface of the silicon layer and is sandwiched between polycarbonate and silicon substrates to facilitate effective coupling of electromagnetic energy between the open-circuited microstrip-line to the patch array. The radiation patches and open-ended microstrip-line are made of Aluminum with conductivity of 3.8×10^7 S/m, thickness of 3 microns and surface roughness of 0.2 microns. Unlike previous antenna designs the proposed technique gets rid of the otherwise bulky structure. Parameters of the metal slot-line and radiation elements were optimized to match with the impedance of the feeding-line in order to achieve high-gain performance over the antenna's sub-THz working band.

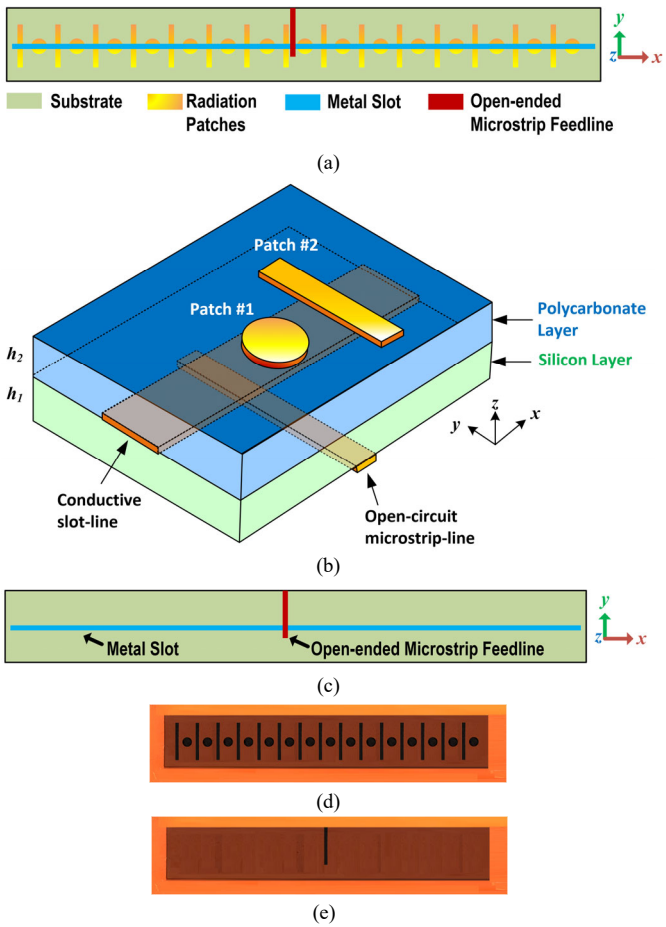

Fig. 1. Silicon-based integrated on-chip antenna, (a) top-side, (b) side-vision with a partially enlarged section, (c) back view, (d) manufactured prototype (top-side), and (e) manufactured prototype (bottom-side). The proposed on-chip antenna has a total dimension of 20×3.5×0.126 mm^3. It is constructed from three different layers, i.e.: (i) polycarbonate, (ii) silicon, and (iii) aluminum.

In the proposed on-chip antenna structure the travelling-wave propagating along the slot-line excites two orthogonal TM_{11} patch modes when the circular-patch is placed on the aperture of the metal slot-line [14]. The two modes have a 90° phase difference because the phase of the electric field is 90° in advance of the current on a resonant patch [15]. As the amplitudes of the two-modes are difficult to control it was necessary to include a linearly polarized rectangular patch. The combination of two different patches generates the required circularly polarized radiation. The phase and axial-ratio of the two orthogonal-modes can be controlled by adjusting two parameters, i.e. the spacing between adjacent pairs of patches and the open-circuit slot line width.

The antenna's reflection-coefficient (S_{11}<-10dB) shown in Fig.2 was determined with two different 3-D full-wave electromagnetic computational techniques (CST Microwave Studio & HFSS). The simulated and measured results show that, the proposed structure operates over the frequency range of 290-316 GHz for S_{11}≤-10dB, which corresponds to an impedance bandwidth of 8.5%. It is noticed that the antenna has a narrow stopband from 292 GHz to 294 GHz, and there is excellent correlation is observed between the two simulation tools. The empirical results in Fig.2 verify the viability of the proposed THz antenna for wideband applications. The discrepancy observed between the measured and simulated results is due to (i) the unknown dielectric loss-tangent over the required frequency range in the foundry's design kit when the 3D model of the antenna was constructed; (ii) manufacturing tolerances; and (iii) feed mismatch losses.

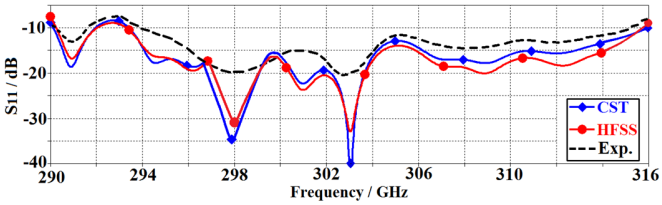

Fig. 2. Simulated and measured reflection coefficient (S_{11}≤-10 dB).

The simulated surface current distribution over the radiation elements at 300 GHz is shown in Fig.3 for different phase angles. It is evident that the rectangular-patches participate towards a *y*-axis polarized radiation, and the circular patches participate towards both *x*- and *y*-axis polarizations, to yield left-handed circularly polarized radiation.

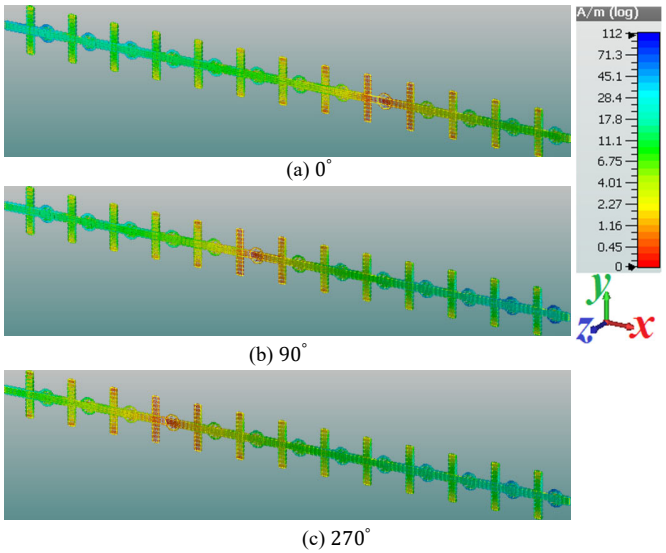

Fig. 3. Surface-current distribution over the radiation elements at 300 GHz for different phase angles.

The antenna's radiation specifications were tested applying a compact antenna test range as illustrated in [16]. The antenna measurement setup with the attached horn antenna on the transmitter is shown in Fig. 4(a). To decrease multipath reflections in the test area, RF absorbing material has utilized to nearly all metallic surfaces and objects on the probe station as shown in Fig. 4(b). A vacuum pump was used to hold down the chip to the rigid microwave absorber while the RF probe touched down. The actual measurements using the standard horn were made from below the AUT in Fig. 4(b). E- and H-planes radiation patterns at the operating frequencies of 295, 300, and 305 GHz are plotted in Figs. 5(a) and (b), respectively. Axial-ratio E-plane of the THz antenna array at various spot frequencies across the antenna's working band are given in Table I. It shows the broadside axial-ratio is maintained under 3dB across the operating frequency range. Gain and radiation efficiency curves throughout the working frequency band is plotted in Fig.6. The radiation efficiency was determined by taking the ratio of the measured radiated power to the input power. The measurement equipment of high thermal stability was carefully calibrated with highly accurate verification standards to minimize errors. Broadside gain and efficiency at 300 GHz are 11.71dBi and 70.8%. Although, because of the characteristics of series fed antenna, when the operating frequency is away from 0.3 THz the beam is tilts slightly and the gain is marginally affected. The 3 dB bandwidth is shown to reduce at frequencies higher than 0.3 THz. The radiation gain and efficiency are also affected by the high conductor and dielectric loss at sub-THz band.

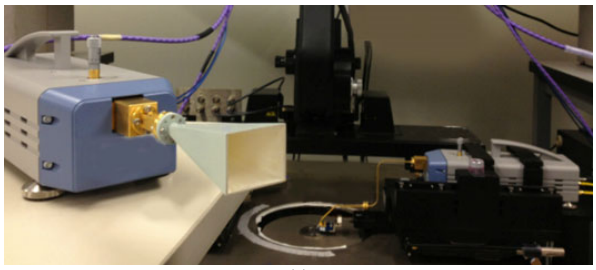

(a)

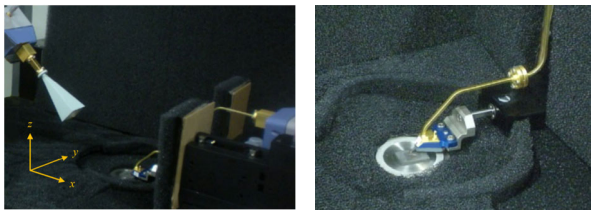

(b)

Fig. 4. (a) Sub-THz antenna measurement setup, and (b) RF absorber material seen as black spongy sheets. The on-chip AUT was located on a Cascade Microtech rigid microwave absorber and probed applying the GSG RF probe. Physical contact was used to connect the ground pads of the GSG probe with the ground plane of the microstrip.

TABLE I. MEASURED AXIAL-RATIO E-PLANE

Frequency (THz)	Axial-ratio E-plane
0.295	1.80
0.3	1.25
0.305	2.30

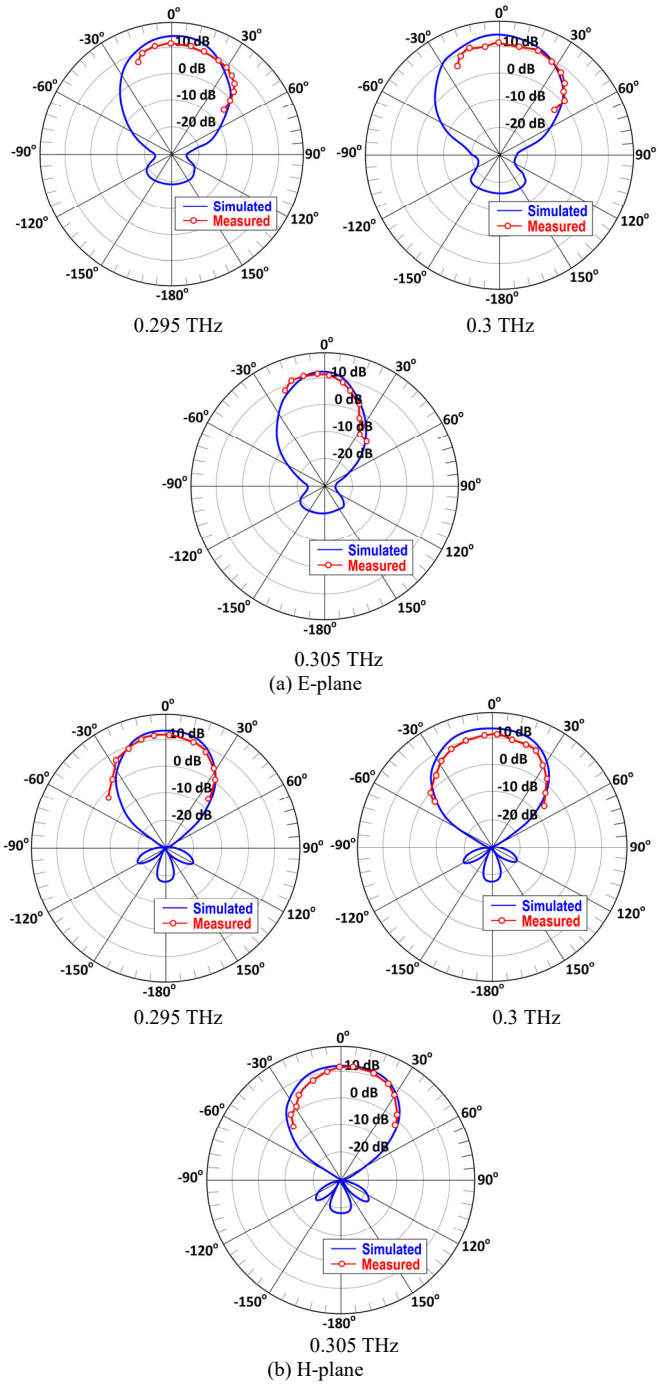

Fig. 5. Radiation patterns at 295 GHz, 300 GHz, and 305 GHz.

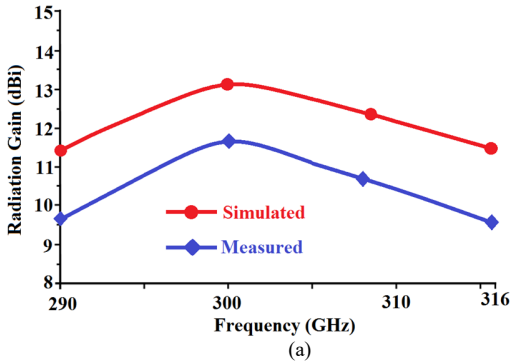

(a)

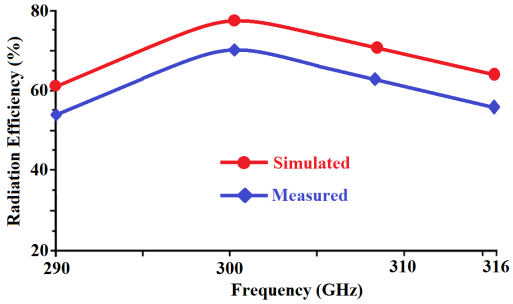

(b)

Fig. 6. (a) Gain, and (b) radiation efficiency as a function of frequency.

Performance parameters of the proposed silicon-based on-chip antenna has compared with recently published millimeter-wave antennas in Table II. It is evident that previous works are based on newer fabrication processes of 0.09-µm, 0.13-µm, and 0.18-µm technologies however in this work the on-chip antenna was fabricated on a standard 120-µm process as the smallest dimension in the design is limited to 200-µm. The purpose of this investigation was to determine by how much we could extend the operating frequency range of a terahertz antenna using the standard silicon technology. Compared to the publications cited it exhibits a higher gain and radiation efficiency. Although its radiation efficiency is lower than [23] that operates at 45-70 GHz however the proposed antenna works at a significantly higher frequency band of 290-316 GHz.

TABLE II. COMPARISON RESULTS

Ref.	**Antenna Type**	**Meas. Freq. Band (GHz)**	**Meas. Gain (dBi)**	**Meas. Eff. (%)**	**Size (mm^3) or (mm^2)**	**Process**
[17]	Bowtie-slot	90-105	≤-1.78	-	0.71×0.31× 0.65	IHP 0.13-µm Bi-CMOS
[18]	Differential-fed Circularly Polarized	50-70	≤-3.2	-	1.5×1.5 ×0.3	0.18-µm
[19]	Ring-shaped Monopole	50-70	≤0.02	≤ 35	-	CMOS 0.18-µm
[20]	Circular Open-loop	57-67	≤ -4.4	-	1.8×1.8 ×0.3	CMOS 0.18-µm
[21]	AMC embedded squared slot antenna	15-66	≤ 2	-	1.44× 1.1	CMOS 0.09-µm
[22]	Monopole	45-70	≤4.96	-	1.9×1.9× 0.25	Silicon CMOS
[23]	Loop Antenna	65-69	≤8	≤96	0.7× 1.25	CMOS 0.18-µm
[24]	Dipole-Antenna	95-102	≤4.8	-	-	Bi-CMOS
[25]	Tab Monopole	45-75	≤0.1	≤42	1.5×1	Standard CMOS Silicon
This work	Coupled Feeding Mechanism	290-316	≥9.6	≥55	20×3.5×0 .126	Standard 120-µm Silicon

III. CONCLUSIONS

Feasibility of an on-chip antenna model is verified for sub-THz applications. The antenna model is implemented on silicon technology for easy on-chip integration. The antenna employs aperture fed mechanism comprising an open-circuited microstrip-line that is electromagnetically coupled to an orthogonal metal slot-line and periodic array of radiating elements. The antenna operates across 0.290 THz to 0.316 THz with an optimum gain of 11.71dBi and radiation efficiency of 70.8% at 0.30 THz, and it radiates circularly polarized energy. The antenna has a narrow stopband between 0.292 THz to 0.294 THz.

ACKNOWLEDGMENTS

This work is partially supported by RTI2018-095499-B-C31, Funded by Ministerio de Ciencia, Innovación y Universidades, Gobierno de España (MCIU/AEI/FEDER,UE), and innovation programme under grant agreement H2020-MSCA-ITN-2016 SECRET-722424, and the financial support from the UK EPSRC under grant EP/E022936/1.

REFERENCES

[1] S. S. Dhillon, et al., "The 2017 terahertz science and technology roadmap," J. Phys. D. Appl. Phys., 50(4), 043001, 2017.
[2] Nagatsuma, T., et al., "Advances in terahertz communications accelerated by photonics," Nat. Photonics, 10, 371–379, 2016.
[3] I. F. Akyildiz, et al., "Terahertz band: Next frontier for wireless communications," Physical Communication, 12, 16-32, 2014.
[4] H. J. Song and T. Nagatsuma, "Present and future of terahertz communications," IEEE Trans. THz Sci. Tech., 1, 256-263, Sep 2011.
[5] Y. Shimada, et al., "Recent research trends of terahertz measurement standards," IEEE Trans. THz Sci. Tech., 5(6), 1166–1172, 2015.
[6] R. Al Hadi, et al., "A 1k-pixel video camera for 0.7-1.1 terahertz imaging applications in 65-nm CMOS," IEEE J. of Solid-State Cir., 47, 2999-3012, 2012.
[7] G. Hanson, "Radiation efficiency of nano-radius dipole antennas in the microwave and far-infrared regimes," IEEE Ant&Prop. Mag. 50, 66-77, 2008.
[8] D.-K. Lee, "Highly sensitive and selective sugar detection by terahertz nano-antennas," Sci. Rep. 5, 15459, 2015.
[9] Feuillet-Palma, et al., "Strong near field enhancement in THz nano-antenna arrays," Sci. Rep. 3, 1361, 2013.
[10] M. Tamagnone, et al., "Analysis and design of THz antennas on plasmonic resonant graphene sheets," J. Appl. Phys., 112(11), 114915, 2012.
[11] M. Dragoman, et al., "Terahertz antenna based on graphene," J. Appl. Phys., 107(10), 104313, 2010.
[12] N. Llombart, et al., "Silicon micromachined lens antenna for THz integrated heterodyne arrays," IEEE Trans. THz Sci. Tech., 3(5), 515-523, 2013.
[13] W. Hou, et al., "A terahertz diagonal multilayer horn antenna based on MEMS technology," IEEE MTT-S IMWS-AMP, Suzhou, 1-3, 2015.
[14] H. Yi, et al., "Antenna array excited by spoof planar plasmonic waveguide," IEEE AWPL, 13,1227-1230, 2014.
[15] J. R. James and P. S. Hall, Handbook of Microstrip Antennas, 1989
[16] C. Liu, X. Wang, "Design and Test of a 0.3 THz Compact Antenna Test Range," PIER Letters, 70, 81–87, 2017.
[17] M. S. Khan, et al., "Design of bowtie-slot on-chip antenna backed with E-shaped FSS at 94 GHz," 10th EuCAP, Davos, 1-3, 2016.
[18] L. Wang and W. Z. Sun, "A 60-GHz differential-fed circularly polarized on-chip antenna based on 0.18-m COMS technology with AMC structure," IET Int. Radar Conf., Hangzhou, 1-4, 2015.
[19] H. T. Huang, et al., "A circular ring-shape monopole on-chip antenna with artificial magnetic conductor," IEEE APMC, 1-3, 2015.
[20] X. Y. Bao, et al., "60-GHz AMC-Based Circularly Polarized On-Chip Antenna Using Standard 0.18-m CMOS Technology," IEEE Trans. on Ant. and Prop., 60(5), 2234-2241, 2012.
[21] F. Lin and B. L. Ooi, "Integrated millimeter-wave on-chip antenna design employing artificial magnetic conductor," IEEE RFIT, pp. 174-177, 2009.
[22] S. Upadhyay and S. Srivastava, "A 60-GHz on-chip monopole antenna using silicon technology," IEEE AEMC, 1-2, 2013.
[23] Y. Song, et al., "The design of a high gain on-chip antenna for SoC application," IEEE MTT-S IMWS-AMP, Suzhou, 1-3, 2015.
[24] M. Nafe, et al., "Gain enhancement of low profile on-chip dipole antenna via Artificial Magnetic Conductor at 94 GHz," 9th EuCAP, 1-3, 2015.
[25] W. Yang, et al., "A 60GHz on-chip antenna in standard CMOS silicon Technology," IEEE APCCAS, Kaohsiung, 252-255, 2012.